Letter

Bubble Magnetometry of Nanoparticle Heterogeneity and Interaction

Andrew L. Balk,[1,2,3] Ian Gilbert,[1] Robert Ivkov,[4] John Unguris,[1] and Samuel M. Stavis[5,*]

[1]*Center for Nanoscale Science and Technology, National Institute of Standards and Technology, Gaithersburg, Maryland 20899, USA*

[2]*Maryland NanoCenter, University of Maryland, College Park, Maryland 20742, USA*

[3]*National High Magnetic Field Laboratory, Los Alamos National Laboratory, Los Alamos, New Mexico 87544, USA*

[4]*Department of Radiation Oncology and Molecular Radiation Sciences, Johns Hopkins University School of Medicine, Baltimore, Maryland 21231, USA*

[5]*Microsystems and Nanotechnology Division, National Institute of Standards and Technology, Gaithersburg, Maryland 20899, USA*

(Received 4 February 2018; revised manuscript received 25 May 2018; published 7 June 2019)

Bubbles have a rich history as transducers in particle-physics experiments. In a solid-state analogue, we use bubble domains in nanomagnetic films to measure magnetic nanoparticles. This technique can determine the magnetic orientation of a single nanoparticle in a fraction of a second and generate a full hysteresis loop in a few seconds. We achieve this high throughput by tuning the nanomagnetic properties of the films, including the Dzyaloshinskii-Moriya interaction, in an application of topological protection from the skyrmion state to a nanoparticle sensor. We develop the technique on nickel-iron nanorods and iron-oxide nanoparticles, which delineate a wide range of properties and applications. Bubble magnetometry enables precise statistical analysis of the magnetic hysteresis of dispersed nanoparticles, and direct measurement of a transition from superparamagnetic behavior as single nanoparticles to collective behavior in nanoscale agglomerates. These results demonstrate a practical capability for measuring the heterogeneity and interaction of magnetic nanoparticles.

DOI: 10.1103/PhysRevApplied.11.061003

I. INTRODUCTION

Nanoscale manipulation is increasingly important in medicine, manufacturing, and sensing [1–3]. In environments where direct contact with a manipulator is undesirable, such as in living beings, nanoparticles enable remote manipulation [4–7]. Magnetic nanoparticles are particularly useful [8–17] due to their biological compatibility, ease of synthesis, and coupling to external fields [9,18,19]. This provides motivation for new measurement technology, as bulk magnetometry [20,21] cannot readily resolve the heterogeneous properties of single nanoparticles, whereas single-particle techniques that are more specialized [22–28] often require meticulous preparation and are impractical for statistical analysis, which is critical for quality control and practical application [29].

Magnetic bubble domains have been demonstrated as field sensors for memory devices [30–32] and for nanoparticle magnetometry [33,34]. However, these recent measurements did not achieve significantly higher throughput or greater sensitivity than other single-particle techniques. Here, we advance bubble magnetometry to measure single nanoparticles in real time, requiring only a few seconds to obtain a full hysteresis loop, which is orders of magnitude faster than other magnetometry techniques [23,27]. In our technique, nanoparticles nucleate bubbles in a nanomagnetic film with perpendicular anisotropy. We expand the bubbles by applying a field of a few millitesla perpendicular to the film, and then measure the bubbles by magneto-optical-Kerr-effect (MOKE) microscopy. The perpendicular anisotropy of the sensor film enables simultaneous and independent modification of the magnetic state of the nanoparticle for hysteresis measurement, in contrast to techniques with higher spatial resolution [35,36].

We tune both the coercive field $\mu_0 H_c$ and the Dzyaloshinskii-Moriya interaction (DMI) of our films to detect millitesla fields over sensor areas of less than 1 μm^2. The DMI provides topological protection from the skyrmion state of the bubbles, increasing the sensitivity and selectivity of bubble nucleation. These improvements enable precise statistical analysis of magnetic hysteresis loops of single dispersed nanoparticles, elucidating the propagation of heterogeneity from dimensional to magnetic property distributions. Furthermore, bubble magnetometry enables direct measurement of the transition in hysteresis from superparamagnetic behavior of

*samuel.stavis@nist.gov

single nanoparticles to collective behavior in agglomerates, which is relevant to cancer hyperthermia.

II. MATERIALS AND METHODS

A. Sensor tuning

Tuning the nanomagnetic properties of trilayer platinum-cobalt-platinum films increases their sensitivity and selectivity for transducing magnetic fields from nanoparticles into bubbles. After growth of the trilayers, we reduce their magnetic anisotropy [37], and thus bubble nucleation energy, by exposure to argon-ion irradiation. For the most sensitive measurements, we spatially vary the exposure dose [33,38,39] to obtain film regions near the spin-reorientation transition [39,40], where the film undergoes a phase transition and therefore has maximal susceptibility. To further increase sensitivity and selectivity, as we discuss below, we tune $\mu_0 H_{\mathrm{DMI}}$ to be negative, by selecting the irradiation energy to be between 80 and 110 eV [41].

B. Sample nanoparticles

Nickel-iron alloy nanorods [33,42] and iron-oxide Johns Hopkins University (JHU) nanoparticles [43] delineate a wide range of relevant properties and uses. Nanorods of similar dimensions are potentially useful for magnetic actuation [44] and superconductivity [45]. JHU nanoparticles are useful for magnetic resonance contrast imaging [46] and magnetic hyperthermia for cancer therapy [47,48]. We initially characterize the samples by scanning electron microscopy (SEM) (see Supplemental Material S1 and S2 [49]). The nanorods are cylindrical, with lengths of 3.9 ± 0.5 μm and diameters of 220 ± 30 nm. Single JHU nanoparticles are aggregates of iron-oxide crystallites, resulting in irregular shapes with approximate diameters of 100 ± 50 nm. Size distributions are mean values $\pm$ standard deviations. Details of sample preparation are in Supplemental Material S3 [49].

C. Signal transduction and amplification

We confirm the process of signal transduction and amplification. After deposition on the film, an anisotropic nanoparticle such as a nanorod with magnetization **M** [Fig. 1(a), red cylinder] generates a fringe field **B** [Fig. 1(a), blue arrows]. **B** can be hundreds of millitesla at the underlying film, nucleating a bubble [Fig. 1(b), white circle] near one of the magnetic poles of the nanorod with zero applied field, $B_{z\,(\mathrm{appl})}$. The pole that nucleates the bubble depends on the relative magnetization directions of the nanorod and the film. We confirm this process by scanning electron microscopy with polarization analysis (SEMPA) [36] [Fig. 1(b), inset]. Subsequent application of $B_{z\,(\mathrm{appl})}$ expands the bubble [Fig. 1(c)], increasing its signal for MOKE microscopy. The center position still indicates the original nucleation position, and therefore the relative

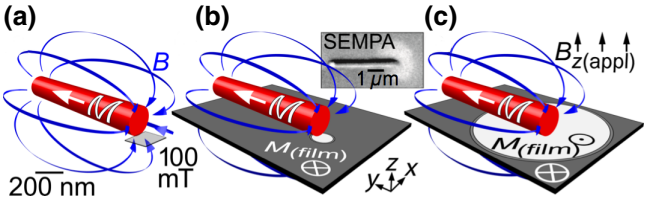

FIG. 1. Magnetic bubbles nucleate and expand underneath a magnetic nanoparticle, amplifying a magneto-optical signal. (a) An anisotropic nanoparticle such as a nanorod (red cylinder) with magnetization **M** produces a fringe field **B** (blue arrows). At the underlying plane, **B** can be hundreds of millitesla. (b) **B** nucleates a bubble (white circle) on a film with magnetization M_{film}. Scanning electron microscopy with polarization analysis (SEMPA) shows a representative nanorod and bubble (inset). (c) Field application in the z direction $B_{z\,(\mathrm{appl})}$ of 5 mT expands the bubble for measurement by MOKE microscopy.

magnetization of the nanorod. The process in Figs. 1(b) and 1(c) is a single amplification cycle.

D. Measurement frequencies

Many measurements per unit field are necessary to obtain hysteresis loops with high resolution. We optimize $B_{z\,(\mathrm{appl})}$ to provide hundreds of amplification cycles per second (see Supplemental Material S4 [49]), and we measure the bubbles at a rate of 20 images per second. Aside from effects of the DMI [50], which we discuss below, in-plane magnetic fields do not influence bubble growth as the film has out-of-plane magnetization. Therefore, we can simultaneously apply an in-plane field $B_{y\,(\mathrm{appl})}$ to modify the magnetic state of a sample nanoparticle. The $B_{y\,(\mathrm{appl})}$ frequency of 50–100 mHz is much lower than the $B_{z\,(\mathrm{appl})}$ and imaging frequencies, so the signal that we measure from the film allows read-out of nanoparticle magnetization in real time.

E. Magnetic orientation and switching

During application of $B_{z\,(\mathrm{appl})}$, bubbles indicating the magnetization direction of each nanorod [Fig. 2(a)] and some of the JHU nanoparticles [Fig. 2(b)] become visible in MOKE micrographs. In Figs. 2(a) and 2(b), the magnetic moment of each sample points in the $+y$ direction, in response to $B_{y\,(\mathrm{appl})} \approx 10$ mT. The JHU nanoparticles themselves are not visible in Fig. 2(b), but we infer their presence from the bubbles that nucleate and expand under them. Subsequent analysis indicates that the film senses only the largest JHU nanoparticles and agglomerates of a few JHU nanoparticles that form after dispersion in aqueous media. When $B_{y\,(\mathrm{appl})}$ sweeps through zero and to -10 mT, the bubbles under the nanorod [Fig. 2(c)] and JHU nanoparticles [Fig. 2(d)] move abruptly, indicating magnetic switching of the particles. We restrict our analysis to binary magnetic switching of nanoparticles,

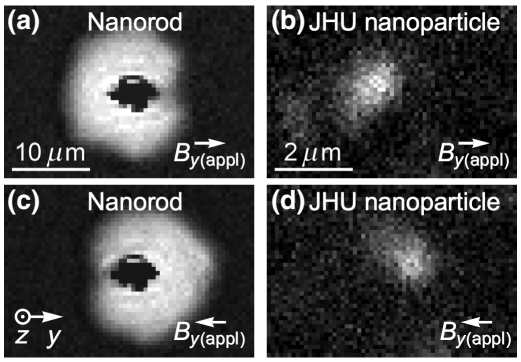

FIG. 2. MOKE micrographs showing bubble positions indicating the relative magnetization of a nickel-iron nanorod and an iron-oxide JHU nanoparticle. (a),(b) With field application in the $+y$ direction, (a) the bubble from the nanorod expands (white shape) around its nucleation position on the left side of the nanorod (central black shape), indicating that the nanorod magnetization **M** is in the $+y$ direction. (b) JHU nanoparticles are not visible but nucleate bubbles, which are visible after expansion (white shape). (c),(d) With field application in the $-y$ direction, (c) the bubble moves to the right side of the nanorod, indicating that **M** has switched to the $-y$ direction. (d) The bubble from the JHU nanoparticle originates farther to the right than the bubble in (b), indicating the switching of **M** to the $-y$ direction. Bright contrast indicates film magnetization in the $+z$ direction. We show images after background subtraction.

assuming that they are single-domain structures, but it is also possible to infer multiple-domain configurations.

F. Hysteresis measurements

A representative video shows magnetic switching of 14 nanorods in real time without image processing (see Supplemental Material S5 [49]). To obtain hysteresis loops from such videos, we extract the bubble position and therefore the relative magnetization **M** of a nanoparticle by convolving each image with a kernel consisting of a positive and a negative Gaussian function on either side of the nanoparticle. Plotting the integral of the convolution as a function of $B_{y\,(\mathrm{appl})}$ yields a hysteresis loop. To extract values of $\mu_0 H_c$, we fit error functions to the hysteresis loops by the method of damped least squares, quantifying uncertainties in determining the point of maximum slope.

III. RESULTS AND DISCUSSION

A. Measurement robustness

Several tests confirm that bubble magnetometry is usefully robust to various measurement parameters and film properties. We measure nanorods with a sinusoidal waveform of $B_{z\,(\mathrm{appl})}$ at a range of frequencies and amplitudes, as well as values of film $\mu_0 H_c$. The values of nanorod $\mu_0 H_c$ that we measure are independent of these parameters within uncertainty (see Supplemental Material S6 [49]), and are also insensitive to small angles between the primary axes of the nanorods and $B_{y\,(\mathrm{appl})}$ (see Supplemental Material S7 [49]).

B. DMI effects

We observe that the DMI has an important effect on bubble nucleation (see Supplemental Material S8 [49]). Briefly, if the effective DMI field $\mu_0 H_{\mathrm{DMI}}$ is negative, then the bubbles have a domain-wall chirality that matches the direction of the stray field from the nanoparticles. This reduces the nucleation energy, effectively encouraging the formation of skyrmions and increasing the sensitivity and selectivity of the film. JHU nanoparticles nucleate bubbles on films only where $\mu_0 H_{\mathrm{DMI}}$ is negative, emphasizing the importance of controlling this property, and marking its first rational design [41] for a nanoparticle sensor. The DMI also results in asymmetric bubble expansion [50], causing a measurement artifact that we characterize in Supplemental Material S8 [49].

C. Nanoparticle hysteresis

We repeat the measurement over many cycles of $B_{y\,(\mathrm{appl})}$ to obtain a series of hysteresis loops of sample nanoparticles, elucidating behavior that would be difficult or impossible to resolve otherwise. Overlaying hysteresis loops of an exemplary nanorod [Fig. 3(a)] shows sharp and repeatable transitions, indicating that these anisotropic nanoparticles have exchange coupling throughout their volume. Some of the JHU nanoparticles have similar values of $\mu_0 H_c$ [Fig. 3(b)], however, the switching fields vary for each field cycle [51]. We observe this behavior for various excitation fields and film properties, indicating that

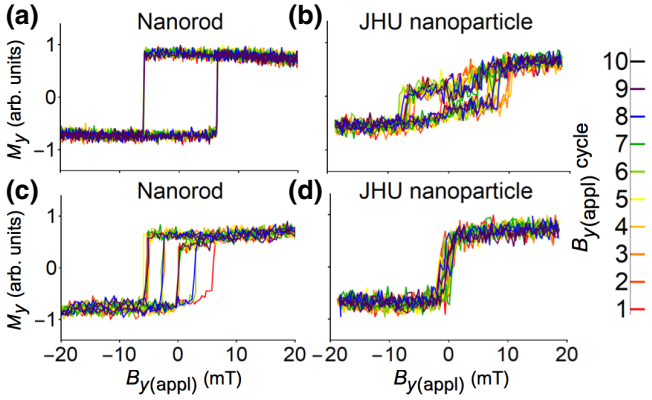

FIG. 3. Variable switching of nickel-iron nanorods and iron-oxide JHU nanoparticles. (a) A nanorod with a large mean $\mu_0 H_c$ switches sharply and consistently. (b) A JHU nanoparticle with several values of $\mu_0 H_c$ that are similar to that of the nanorod in (a) switches stochastically. (c) A nanorod with a smaller mean $\mu_0 H_c$ shows several different values of $\mu_0 H_c$ from consecutive measurements. (d) A JHU nanoparticle with a smaller mean $\mu_0 H_c$ shows the onset of superparamagnetism.

the measurement is sensitive to stochastic switching of the nanoparticles. Furthermore, some of the nanorods with smaller values of $\mu_0 H_c$ show similar behavior [Fig. 3(c)], and JHU nanoparticles with small values of $\mu_0 H_c$ have switching fields that vary by amounts approaching this value [Fig. 3(d)], indicating the onset of superparamagnetism. This unique capability of resolving the switching-field distribution from thermal fluctuations, for many dispersed nanoparticles, allows estimation of the mean energy barrier for magnetic switching. Applying a Néel-Brown model and estimating the effective anisotropy fields H_k [51,52], we calculate energy barriers of approximately 0.8 eV for the nanorods and approximately 0.1 eV for the JHU nanoparticles.

D. Statistical analysis

The high throughput of bubble magnetometry allows measurement of hundreds of nanorods [Fig. 4(a)] and JHU nanoparticles [Fig. 4(b)]. This is an order of magnitude more than in previous studies [23,26,27], enabling precise analysis of property distributions. For the nanorods, some of the hysteresis loops are noisier due to a higher $\mu_0 H_c$ of the film, and DMI biases are evident in some of the hysteresis loops, but neither affects the $\mu_0 H_c$ values of the nanorods that we measure (see Supplemental Material S6 [49] and Fig. 4). Most of the hysteresis loops have single, sharp transitions [Fig. 4(a), gray circle]. Such hysteresis loops are from approximately cylindrical nanorods [Fig. 4(c), left inset]. A few of the hysteresis loops [Fig. 4(a), black circle] show multiple, distinct switching events, from nanorods in bundles or with irregular shapes [Fig. 4(c), right inset and Supplemental Material S1 [49]]. This highlights the utility of bubble magnetometry to resolve heterogeneous magnetic properties, which are sensitive to nanoscale variation in structure. The nanorods have a mean $\mu_0 H_c$ of 7.2 mT and a standard deviation of 5.7 mT [Fig. 4(c)], with a mean standard uncertainty of approximately 0.3 mT. We observe a correlation between mean $\mu_0 H_c$ and length (see Supplemental Material S1 [49]) with R^2

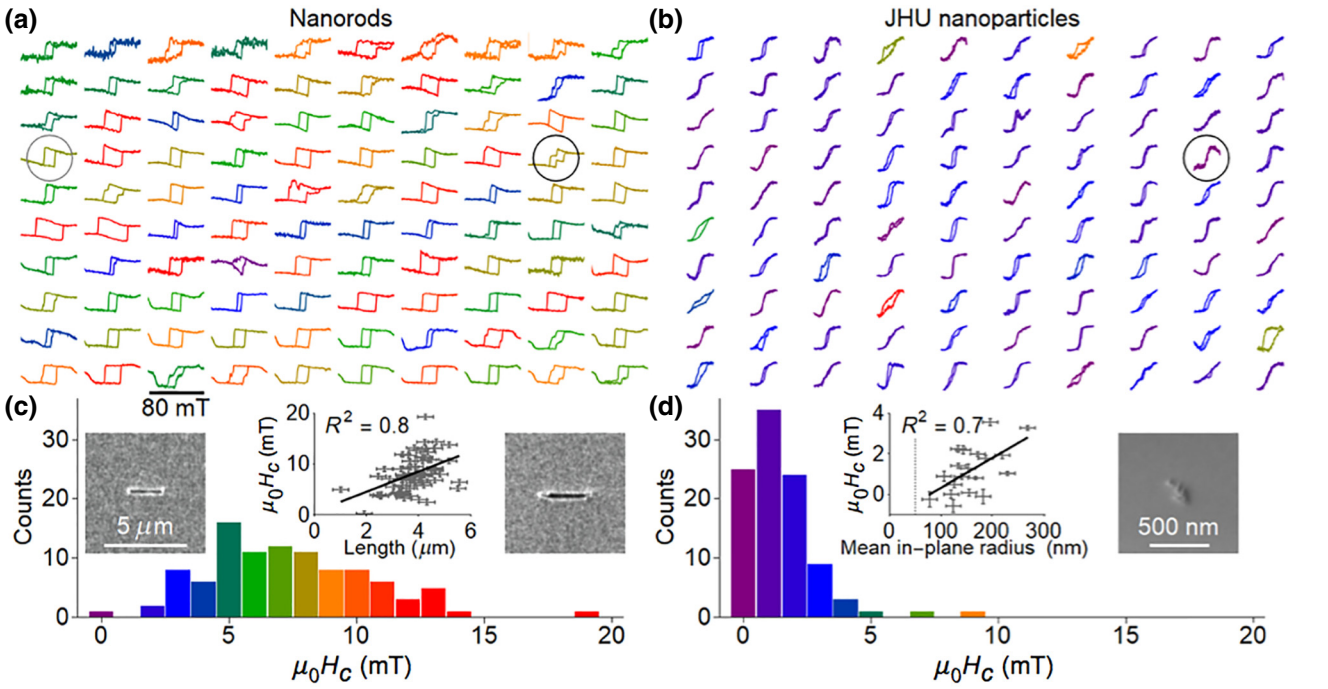

FIG. 4. Bubble magnetometry enables statistical analysis of nanoparticles. (a) Hysteresis loops of nickel-iron nanorods with colors corresponding to $\mu_0 H_c$ values. The range of the y axis is arbitrary. (b) Hysteresis loops of iron-oxide JHU nanoparticles, with the same $B_{y\,(\mathrm{appl})}$ and color scale as in (a). (c) A $\mu_0 H_c$ histogram of the nanorods shows a mean of 7.2 mT and a standard deviation of 5.7 mT. The inset graph shows correlation of mean $\mu_0 H_c$ and nanorod length, showing the influence of shape anisotropy. The inset images show SEM micrographs of a cylindrical nanorod (left) and a nanorod bundle (right), corresponding, respectively, to the hysteresis loops with gray and black circles in (a). (d) A $\mu_0 H_c$ histogram of the JHU nanoparticles shows a mean of 2.2 mT and a standard deviation of 3.0 mT. The inset graph shows correlation of mean $\mu_0 H_c$ and mean in-plane radius of JHU nanoparticles and agglomerates. Extrapolation (solid black line) to the mean radius of single JHU nanoparticles (dash gray line) shows that many JHU nanoparticles have vanishing $\mu_0 H_c$, thus exhibiting superparamagnetic behavior at measurement frequencies of less than 1 Hz. Negative values of $\mu_0 H_c$ could result from stochastic switching. The inset image shows a SEM micrograph of the smallest measurable JHU nanoparticle, corresponding to the hysteresis loop with a circle in (b). In both inset graphs, vertical bars are standard uncertainties and horizontal bars are limits of uncertainty (see Supplemental Material S1 and S2 [49]).

of 0.8 [Fig. 4(c), inset graph], which is consistent with a significant influence of shape anisotropy on magnetic properties. In comparison, the JHU nanoparticles typically have smaller $\mu_0 H_c$, with a mean of 2.2 mT and a standard deviation of 3.0 mT, with a mean standard uncertainty of 0.5 mT. Furthermore, the smaller JHU nanoparticles all switch stochastically to some extent, due to the increasing importance of thermal effects on their magnetic properties.

E. Nanoparticle superparamagnetism

For the JHU nanoparticles, many $\mu_0 H_c$ values approach 0 mT, so we hypothesize that some particles are superparamagnetic under our measurement conditions. To test this, we characterize a subset by SEM to determine their in-plane sizes (see Supplemental Material S2 [49]). The results are consistent with those of a previous study [43], although we observe larger particles with a greater variety of shapes, indicating that this subset ranges from single JHU nanoparticles near the large end of their size distribution to agglomerates of a few JHU nanoparticles. The mean $\mu_0 H_c$ of these nanoparticles or agglomerates correlates with their mean in-plane radius [Fig. 4(d), inset graph], with R^2 of 0.7. Extrapolation of this trend to the mean radius of single JHU nanoparticles of approximately 50 nm [Fig. 4(d) inset graph, dash gray line] shows that many have vanishing $\mu_0 H_c$ and therefore are superparamagnetic at our measurement frequency of less than 1 Hz. From the smallest measurable JHU nanoparticle [Fig. 4(d), hysteresis loop in black circle and inset image], we estimate the moment sensitivity of our technique as 5×10^{-16} A m^2. This compares favorably with direct Kerr magnetometry which can obtain slightly better sensitivity [53], with lower throughput and the requirement of reflective samples.

F. Agglomerate behavior

Exchange coupling between JHU nanoparticles in an agglomerate is unlikely, and the largest particles that we measure from this sample are larger than we expect for the population [43]. Therefore, the correlation of $\mu_0 H_c$ and the mean in-plane radius, for radii larger than single JHU nanoparticles, indicates that nanoparticle fringe fields mediate their collective behavior, resulting in a superferromagnetic or a superspin glass state within agglomerates [54]. In these states, single nanoparticles are superparamagnetic but dipolar interactions cause collective behavior, leading to magnetic hysteresis of agglomerates [55]. Previous studies reported evidence of such behavior in ensemble measurements of nanoparticles in granular films [56–58], two-dimensional arrays [59,60], and quasi-two-dimensional and one-dimensional chains [61]. In comparison, bubble magnetometry enables the direct measurement of the transition in hysteresis from superparamagnetic behavior of single nanoparticles to their collective behavior in nanoscale agglomerates. This result emphasizes the importance of isolating nanoparticle interactions, which can confound ensemble magnetometry and affect nanoparticle function in critical applications. In particular, nanoparticles commonly agglomerate in biological media [62,63], and their resulting properties strongly influence heating efficiency [64] in cancer hyperthermia. Future measurements at higher frequencies will further elucidate such structure-property relationships.

IV. CONCLUSION

We report a magnetometry technique that applies the nucleation and expansion of bubble domains to generate hysteresis loops of single nanoparticles in a few seconds. This is orders of magnitude faster than previously reported techniques. We achieve this high throughput by tuning the nanomagnetic properties of our sensor films, including the rational design of the DMI for such devices. This enables application of this technique to elucidate the physical properties of dispersed nanoparticles, including their heterogeneity and interaction. Bubble magnetometry can facilitate fundamental study of magnetic nanoparticles, and also meet the critical challenge of statistical analysis for quality control [29]. This will enable emerging technologies that rely on magnetic nanoparticles [45,47], and foster further development of technology for measurement [34,65] and application of magnetic nanoparticles.

ACKNOWLEDGMENTS

The authors acknowledge Emily Follansbee for assistance with figure preparation, Lamar Mair and Carlos Hangarter for assistance with sample preparation, and Mark Stiles for helpful comments. A.L.B. acknowledges support of this research under the Cooperative Research Agreement between the University of Maryland and the National Institute of Standards and Technology Center for Nanoscale Science and Technology (Award No. 70NANB10H193) through the University of Maryland.

[1] M. Sitti, Microscale and nanoscale robotics systems [grand challenges of robotics], Robotics & Automation Magazine, IEEE **14**, 53 (2007).
[2] L. Ricotti and A. Menciassi, Nanotechnology in biorobotics: opportunities and challenges, J. Nanopart. Res. **17**, 1 (2015).
[3] R. A. Freitas, Current status of nanomedicine and medical nanorobotics, J. Comput. Theor. Nanosci. **2**, 1 (2005).
[4] A. Cavalcanti, B. Shirinzadeh, and L. C. Kretly, Medical nanorobotics for diabetes control, Nanomed.: Nanotech., Biol. Med. **4**, 127 (2008).
[5] C. Lee, H. Lee, and R. Westervelt, Microelectromagnets for the control of magnetic nanoparticles, Appl. Phys. Lett. **79**, 3308 (2001).

[6] L. O. Mair, B. A. Evans, A. Nacev, P. Y. Stepanov, R. Hilaman, S. Chowdhury, S. Jafari, W. Wang, B. Shapiro, and I. N. Weinberg, Magnetic microkayaks: propulsion of microrods precessing near a surface by kilohertz frequency, rotating magnetic fields, Nanoscale **9**, 3375 (2017).

[7] M. Donolato, P. Antunes, R. S. Bejhed, T. Z. G. de la Torre T, F. W. Østerberg, M. Strömberg, M. Nilsson, M. Strømme, P. Svedlindh, M. F. Hansen, and P. Vavassori, Novel readout method for molecular diagnostic assays based on optical measurements of magnetic nanobead dynamics, Anal. Chem. **87**, 1622 (2015).

[8] J.-P. Fortin, C. Wilhelm, J. Servais, C. Ménager, J.-C. Bacri, and F. Gazeau, Size-sorted anionic iron oxide nanomagnets as colloidal mediators for magnetic hyperthermia, J. Am. Chem. Soc. **129**, 2628 (2007).

[9] C. Grüttner, K. Müller, J. Teller, F. Westphal, A. Foreman, and R. Ivkov, Synthesis and antibody conjugation of magnetic nanoparticles with improved specific power absorption rates for alternating magnetic field cancer therapy, J. Magn. Magn. Mater. **311**, 181 (2007).

[10] E. Cespedes, J. M. Byrne, N. Farrow, S. Moise, V. S. Coker, M. Bencsik, J. R. Lloyd, and N. D. Telling, Bacterially synthesized ferrite nanoparticles for magnetic hyperthermia applications, Nanoscale **6**, 12958 (2014).

[11] B. B. Yellen, O. Hovorka, and G. Friedman, Arranging matter by magnetic nanoparticle assemblers, Proc. Natl. Acad. Sci. U. S. A. **102**, 8860 (2005).

[12] Y. Zhao, J. Fang, H. Wang, X. Wang, and T. Lin, Magnetic liquid marbles: manipulation of liquid droplets using highly hydrophobic Fe_3O_4 nanoparticles, Adv. Mater **22**, 707 (2010).

[13] Y. Cheng, M. E. Muroski, D. C. M. C. Petit, R. Mansell, T. V. Ramin, A. Morshed, Y. Han, I. V. Balyasnikova, C. M. Horbinski, X. Huang, L. Zhang, R. P. Cowburn, and M. S. Lesniaka, Rotating magnetic field induced oscillation of magnetic particles for in vivo mechanical destruction of malignant glioma, J. Control. Release **223**, 75 (2016).

[14] A. Tay and D. Di Carlo, Magnetic nanoparticle-based mechanical stimulation for restoration of mechanosensitive ion channel equilibrium in neural networks, Nano Lett. **17**, 886 (2017).

[15] B. Polyak, I. Fishbein, M. Chorny, I. Alferiev, D. Williams, B. Yellen, G. Friedman, and R. J. Levy, High field gradient targeting of magnetic nanoparticle-loaded endothelial cells to the surfaces of steel stents, Proc. Natl. Acad. Sci. U. S. A. **105**, 698 (2008).

[16] B. A. Moffat, G. R. Reddy, P. McConville, D. E. Hall, T. L. Chenevert, R. R. Kopelman, M. Philbert, R. Weissleder, A. Rehemtulla, and B. D. Ross, A novel polyacrylamide magnetic nanoparticle contrast agent for molecular imaging using MRI, Mol. Imaging **2**, 324 (2003).

[17] J.-P. Cleuziou, W. Wernsdorfer, T. Ondarçuhu, and M. Monthioux, Electrical detection of individual magnetic nanoparticles encapsulated in carbon nanotubes, ACS Nano **5**, 2348 (2011).

[18] L. Wang, J. Bao, L. Wang, F. Zhang, and Y. Li, One-pot synthesis and bioapplication of amine-functionalized magnetite nanoparticles and hollow nanospheres, Chem. Eur. J. **12**, 6341 (2006).

[19] J.-F. Lutz, S. Stiller, A. Hoth, L. Kaufner, U. Pison, and R. Cartier, One-pot synthesis of PEGylated ultrasmall iron-oxide nanoparticles and their in vivo evaluation as magnetic resonance imaging contrast agents, Biomacromolecules **7**, 3132 (2006).

[20] D. Eberbeck, F. Wiekhorst, U. Steinhoff, and L. Trahms, Aggregation behaviour of magnetic nanoparticle suspensions investigated by magnetorelaxometry, J. Phys. Cond. Mat. **18**, S2829 (2006).

[21] J. Chatterjee, Y. Haik, and C.-J. Chen, Polyethylene magnetic nanoparticle: a new magnetic material for biomedical applications, J. Magn. Magn. Mater **246**, 382 (2002).

[22] W. Wernsdorfer, D. Mailly, and A. Benoit, Single nanoparticle measurement techniques, J. Appl. Phys. **87**, 5094 (2000).

[23] D. P. Weber, D. Rüffer, A. Buchter, F. Xue, E. Russo-Averchi, R. Huber, P. Berberich, J. Arbiol, A. Fontcuberta i Morral, D. Grundler, and M. Poggio, Cantilever magnetometry of individual Ni nanotubes, Nano Lett. **12**, 6139 (2012).

[24] M. Jamet, W. Wernsdorfer, C. Thirion, D. Mailly, V. Dupuis, P. Mélinon, and A. Pérez, Magnetic Anisotropy of a Single Cobalt Nanocluster, Phys. Rev. Lett. **86**, 4676 (2001).

[25] D. Schmid-Lorch, T. Häberle, F. Reinhard, A. Zappe, M. Slota, L. Bogani, A. Finkler, and J. Wrachtrup, Relaxometry and dephasing imaging of superparamagnetic magnetite nanoparticles using a single qubit, Nano Lett. **15**, 4942 (2015).

[26] B. Stipe, H. Mamin, T. Stowe, T. Kenny, and D. Rugar, Magnetic Dissipation and Fluctuations in Individual Nanomagnets Measured by Ultrasensitive Cantilever Magnetometry, Phys. Rev. Lett. **86**, 2874 (2001).

[27] F. Kronast, N. Friedenberger, K. Ollefs, S. Gliga, L. Tati-Bismaths, R. Thies, A. Ney, R. Weber, C. Hassel, F. M. Römer, A. V. Trunova, C. Wirtz, R. Hertel, H. A. Dürr, and M. Farle, Element-specific magnetic hysteresis of individual 18 nm Fe nanocubes, Nano Lett. **11**, 1710 (2011).

[28] S. K. Piotrowski, M. F. Matty, and S. A. Majetich, Magnetic fluctuations in individual superparamagnetic particles, IEEE Trans. Magn. **50**, 1 (2014).

[29] S. M. Stavis, J. A. Fagan, M. Stopa, and J. A. Liddle, Nanoparticle manufacturing – heterogeneity through processes to products, ACS Appl. Nano Mater. **1**, 4358 (2018).

[30] H. Awano, S. Ohnuki, H. Shirai, N. Ohta, A. Yamaguchi, S. Sumi, and K. Torazawa, Magnetic domain expansion readout for amplification of an ultra high density magneto-optical recording signal, Appl. Phys. Lett. **69**, 4257 (1996).

[31] H. Awano, S. Imai, M. Sekine, M. Tani, N. Ohta, K. Mitani, N. Takagi, H. Noguchi, and M. Kume, 20 nm domain expansion readout by magnetic amplifying MO system (MAMMOS), IEEE Trans. Magn. **36**, 2261 (2000).

[32] C. A. Verschuren and H. W. v. Kesteren, Asymmetric run length constraints for increased resolution and power margin in MAMMOS readout, Trans. Magn. Soc. Jpn. **2**, 308 (2002).

[33] A. L. Balk, C. Hangarter, S. M. Stavis, and J. Unguris, Magnetometry of single ferromagnetic nanoparticles using

magneto-optical indicator films with spatial amplification, Appl. Phys. Lett. **106**, 112402 (2015).

[34] J. Wells, A. F. Scarioni, H. W. Schumacher, D. Cox, R. Mansell, R. Cowburn, and O. Kazakova, Detection of individual iron-oxide nanoparticles with vertical and lateral sensitivity using domain wall nucleation in CoFeB/Pt nanodevices, AIP Adv. **7**, 056715 (2017).

[35] E. Snoeck, R. E. Dunin-Borkowski, F. Dumestre, P. Renaud, C. Amiens, B. Chaudret, and P. Zurcher, Quantitative magnetization measurements on nanometer ferromagnetic cobalt wires using electron holography, Appl. Phys. Lett. **82**, 88 (2003).

[36] M. R. Scheinfein, J. Unguris, M. H. Kelley, D. T. Pierce, and R. J. Celotta, Scanning electron microscopy with polarization analysis (SEMPA), Rev. Sci. Instrum. **61**, 2501 (1990).

[37] C. Chappert, H. Bernas, J. Ferré, V. Kottler, J.-P. Jamet, Y. Chen, E. Cambril, T. Devolder, F. Rousseaux, V. Mathet, and H. Launois, Planar patterned magnetic media obtained by ion irradiation, Science **280**, 1919 (1998).

[38] A. Balk, M. Stiles, and J. Unguris, Critical behavior of zero-field magnetic fluctuations in perpendicularly magnetized thin films, Phys. Rev. B **90**, 184404 (2014).

[39] A. L. Balk, F. Li, I. Gilbert, J. Unguris, N. A. Sinitsyn, and S. A. Crooker, Broadband Spectroscopy of Thermodynamic Magnetization Fluctuations through a Ferromagnetic Spin-Reorientation Transition, Phys. Rev. X **8**, 031078 (2018).

[40] J.-W. Lee, J.-R. Jeong, S.-C. Shin, J. Kim, and S.-K. Kim, Spin-reorientation transitions in ultrathin Co films on Pt (111) and Pd (111) single-crystal substrates, Phys. Rev. B **66**, 172409 (2002).

[41] A. L. Balk, K. W. Kim, D. T. Pierce, M. D. Stiles, J. Unguris, and S. M. Stavis, Simultaneous Control of the Dzyaloshinskii-Moriya Interaction and Magnetic Anisotropy in Nanomagnetic Trilayers, Phys. Rev. Lett. **119**, 077205 (2017).

[42] A. L. Balk, L. O. Mair, F. Guo, C. Hangarter, P. P. Mathai, R. D. McMichael, S. M. Stavis, and J. Unguris, Quantitative magnetometry of ferromagnetic nanorods by microfluidic analytical magnetophoresis, J. Appl. Phys. **118**, 093904 (2015).

[43] C. L. Dennis, K. L. Krycka, J. A. Borchers, R. D. Desautels, J. van Lierop, N. F. Huls, A. J. Jackson, C. Gruettner, and R. Ivkov, Internal magnetic structure of nanoparticles dominates time-dependent relaxation processes in a magnetic field, Adv. Funct. Mater. **25**, 4300 (2015).

[44] P. Vavassori, M. Pancaldi, M. J. Perez-Roldan, A. Chuvilin, and A. Berger, Remote magnetomechanical nanoactuation, Small **12**, 1013 (2016).

[45] I. Lyuksyutov, Magnetic nanorod—superconductor hybrids, J. Supercond. Nov. Magn. **23**, 1047 (2010).

[46] M. Wabler, W. Zhu, M. Hedayati, A. Attaluri, H. Zhou, J. Mihalic, A. Geyh, T. L. DeWeese, R. Ivkov, and Dmitri Artemov, Magnetic resonance imaging contrast of iron oxide nanoparticles developed for hyperthermia is dominated by iron content, Int. J. Hyperthermia **30**, 192 (2014).

[47] A. Jordan, R. Scholz, K. Maier-Hauff, M. Johannsen, P. Wust, J. Nadobny, H. Schirra, H. Schmidt, S. Deger, S. Loening, W. Lanksch, and R. Felix, Presentation of a new magnetic field therapy system for the treatment of human solid tumors with magnetic fluid hyperthermia, J. Magn. Magn. Mater. **225**, 118 (2001).

[48] C. L. Dennis, A. J. Jackson, J. A. Borchers, P. J. Hoopes, R. Strawbridge, A. R. Foreman, J. van Lierop, C. Grüttner, and R. Ivkov, Nearly complete regression of tumors via collective behavior of magnetic nanoparticles in hyperthermia, Nanotechnology **20**, 395103 (2009).

[49] See Supplemental Material at http://link.aps.org/supplemental/10.1103/PhysRevApplied.11.061003 for SEM micrographs of nanoparticles, details of sample preparation and field excitation, a video of bubble magnetometry, an analysis of measurement robustness, and a discussion of DMI effects.

[50] S.-G. Je, D.-H. Kim, S.-C. Yoo, B.-C. Min, K.-J. Lee, and S.-B. Choe, Asymmetric magnetic domain-wall motion by the Dzyaloshinskii-Moriya interaction, Phys. Rev. B **88**, 214401 (2013).

[51] W. Wernsdorfer, E. B. Orozco, K. Hasselbach, A. Benoit, B. Barbara, N. Demoncy, A. Loiseau, H. Pascard, and D. Mailly, Experimental Evidence of the Néel-Brown Model of Magnetization Reversal, Phys. Rev. Lett. **78**, 1791 (1997).

[52] D. B. Gopman, D. Bedau, G. Wolf, S. Mangin, E. E. Fullerton, J. A. Katine, and A. D. Kent, Temperature dependence of the switching field in all-perpendicular spin-valve nanopillars, Phys. Rev. B **88**, 100401 (2013).

[53] E. Nikulina, O. Idigoras, P. Vavassori, A. Chuvilin, and A. Berger, Magneto-optical magnetometry of individual 30 nm cobalt nanowires grown by electron beam induced deposition, Appl. Phys. Lett. **100**, 142401 (2012).

[54] B. Subhankar and K. Wolfgang, Supermagnetism, J. Phys. D: Appl. Phys. **42**, 013001 (2009).

[55] R. Cowburn, A. Adeyeye, and M. Welland, Controlling magnetic ordering in coupled nanomagnet arrays, New J. Phys. **1**, 16 (1999).

[56] A. A. Timopheev, V. M. Kalita, S. M. Ryabchenko, A. F. Lozenko, P. A. Trotsenko, A. V. Los, and M. Munakata, Coercivity anomaly in the superferromagnetic state of an ensemble of nanoparticles with oriented anisotropy, J. Appl. Phys. **108**, 053902 (2010).

[57] O. Petracic, X. Chen, S. Bedanta, W. Kleemann, S. Sahoo, S. Cardoso, and P. P. Freitas, Collective states of interacting ferromagnetic nanoparticles, J. Magn. Magn. Mater. **300**, 192 (2006).

[58] M. Vomir, R. Turnbull, I. Birced, P. Parreira, D. A. MacLaren, S. L. Lee, P. André, and J.-Y. Bigot, Dynamical torque in $Co_xFe_{3-x}O_4$ nanocube thin films characterized by femtosecond magneto-optics: A π-shift control of the magnetization precession, Nano Lett. **16**, 5291 (2016).

[59] K. Yamamoto, C. R. Hogg, S. Yamamuro, T. Hirayama, and S. A. Majetich, Dipolar ferromagnetic phase transition in Fe_3O_4 nanoparticle arrays observed by Lorentz microscopy and electron holography, Appl. Phys. Lett. **98**, 072509 (2011).

[60] V. F. Puntes, P. Gorostiza, D. M. Aruguete, N. G. Bastus, and A. P. Alivisatos, Collective behaviour in two-dimensional cobalt nanoparticle assemblies observed

by magnetic force microscopy, Nat. Mater. **3**, 263 (2004).

[61] M. Varón, M. Beleggia, T. Kasama, R. J. Harrison, R. E. Dunin-Borkowski, V. F. Puntes, and C. Frandsen, Dipolar magnetism in ordered and disordered low-dimensional nanoparticle assemblies, Sci. Rep. **3**, 1234 (2013).

[62] A. Giustini, R. Ivkov, and P. Hoopes, Magnetic nanoparticle biodistribution following intratumoral administration, Nanotechnol. **22**, 345101 (2011).

[63] D. Soukup, S. Moise, E. Céspedes, J. Dobson, and N. D. Telling, In situ measurement of magnetization relaxation of internalized nanoparticles in live cells, ACS Nano **9**, 231 (2015).

[64] L. C. Branquinho, M. S. Carrião, A. S. Costa, N. Zufelato, M. H. Sousa, R. Miotto, R. Ivkov, and A. F. Bakuzis, Effect of magnetic dipolar interactions on nanoparticle heating efficiency: Implications for cancer hyperthermia, Sci. Rep. **3**, 2887 (2013).

[65] O. L. Ermolaeva and V. L. Mironov, Domain wall nucleation in ferromagnetic nanowire with perpendicular magnetization stimulated by stray field of V-shaped magnetic particle, IEEE Trans. Magn. **54**, 1 (2018).